Numerical Simulation of the Explosion Dynamics and Energy Release from High-Gain ICF Targets

J.J. MacFarlane, M.E. Sawan, G.A. Moses, P. Wang, R.E. Olson

June 1996

UWFDM-1029

Presented at the 12th Topical Meeting on the Technology of Fusion Power, 16–20 June 1996, Reno NV.

FUSION TECHNOLOGY INSTITUTE

UNIVERSITY OF WISCONSIN

MADISON WISCONSIN

NUMERICAL SIMULATION OF THE EXPLOSION DYNAMICS AND ENERGY RELEASE FROM HIGH-GAIN ICF TARGETS

J. J. MacFarlane, M. E. Sawan, G. A. Moses, P. Wang
Fusion Technology Institute
University of Wisconsin-Madison
Madison, WI 53706-1687
(608) 263-8485

R. E. Olson
Sandia National Laboratories
P. O. Box 5800
Albuquerque, NM 87185
(505) 845-7527

ABSTRACT

Results from numerical simulations are presented describing the explosion energetics of a high-gain indirect-drive ICF target. The light ion fusion LIBRA-SP target, which consists of an x-ray driven capsule embedded in a spherical foam-filled hohlraum, is imploded using 12 prepulse and 12 full power Li beams containing a total energy of 8 MJ. Here, we report on the dynamics of the target energy release, focussing in particular on the partitioning of energy between x rays, neutrons, and target debris kinetic energy. Our results indicate that 72% and 22% of the 552 MJ yield is emitted by the target in the form of neutrons and x-rays, respectively. Calculated emergent spectra for the target neutrons and x rays are also presented.

I. INTRODUCTION

The design of target chambers for high-gain inertial confinement fusion (ICF) facilities will require realistic predictions of the energy release from targets with fusion yields of $\sim 10^2 - 10^3$ MJ. To achieve ignition and a significant burn fraction, the DT fuel must be compressed to densities $\sim 10^3$ g/cm^3, and attain a central "hot spot" temperature of $T > 5$ keV. During the DT fusion burn, 14.1 MeV neutrons and 3.5 MeV α particles are released. The α particles are predominantly reabsorbed in the target. Since about 80% of the energy released during each DT fusion reaction is in the form of 14.1 MeV neutrons, it is important to determine what fraction of their energy is reabsorbed by the target, as well as how the neutron spectrum is softened as the neutrons are scattered by the target. Energy reabsorbed in the target is later reradiated as x rays, as well as converted into kinetic energy of the target debris. Understanding the partitioning of the energy released by the target into x rays, neutrons, and target debris is essential for proper design of ICF reactor chambers.

To study this, we have performed 1-D radiation-hydrodynamics simulations of the explosion dynamics of the light ion-driven LIBRA-SP target.[1] LIBRA-SP[2] is a conceptual light ion ICF reactor study which utilizes self-pinch transport[3] of 24 Li ion beams (12 prepulse and 12 full power) to the target. The LIBRA-SP target is based on the indirect-drive approach; but unlike indirect-drive laser- and heavy ion-driven targets, light ion targets utilize *spherical* hohlraums. In this concept, the x-ray driven ICF capsule is embedded within a spherical foam-filled hohlraum. The Li ions penetrate the hohlraum wall (or radiation case) and deposit the bulk of their energy in a low density CH foam, which converts the ion beam energy into x rays that have a high enough energy to freely traverse the foam and provide the drive for the capsule implosion. Details of this target concept, together with descriptions of recent proof-of-principle experiments for light ion-driven hohlraums and x-ray pulse-shaping techniques, have been presented elsewhere.[1,4]

In this paper, we present results describing the dynamics of the explosion and energy release from the LIBRA-SP target. In particular, we examine the partitioning of the target energy between x rays, neutrons, and target debris kinetic energy. To study this, numerical simulations were performed using the 1-D radiation-hydrodynamics code BUCKY-1.[5] In addition, detailed neutron transport calculations were performed with ONEDANT[6] using density and neutron source profiles computed from the BUCKY-1 simulations. This allows for making detailed predic-

tions of the emergent neutron and gamma spectra. It also provides an accurate benchmark of the neutron energy deposition in the target which can be compared with more approximate escape probability calculations within BUCKY-1.

II. PHYSICS MODELS

The simulation of the implosion, fusion burn, and breakup of the LIBRA-SP target have been performed using the 1-D radiation-hydrodynamics code BUCKY-1.[5] BUCKY-1 is a descendent of the PHD-IV[7] target physics code and the MF-FIRE[8] and CONRAD[9] ICF target chamber codes. It is a 1-D Lagrangian code which solves the single-fluid equation of motion with pressure contributions from electrons, ions, radiation, and fast charged particle reaction products. Energy transfer in the plasma is treated with a 2-temperature model — i.e., separate ion and electron temperatures. Thermal conduction through each species is treated using Spitzer's form of the thermal conductivity. The electron conductivity is flux-limited. Radiation emission and absorption terms couple the electron temperature equation to the radiation transport equations. In addition, the electron and ion temperature equations contain source terms that couple them to the ion beam or laser beam energy deposition calculation and the energy deposited from the fusion reactions. The fusion reaction products are transported and slowed using a time-dependent particle tracking algorithm.

In the simulations described below, SESAME[10] equations of state were used, while multigroup opacities were generated using EOSOPA.[11] EOSOPA includes opacity contributions from bound-bound, bound-free, and free-free transitions. It utilizes a detailed term accounting (DTA) model for low-Z atomic systems, and an unresolved transition array (UTA) model for high-Z systems. Radiation transport was calculated using a diffusion model with 100 frequency groups. The time-dependent radiation energy density equations are solved using implicit finite difference techniques.

III. RADIATION-HYDRODYNAMICS RESULTS

The initial state of the LIBRA-SP target is shown in Fig. 1. It consists of an outer 10 μm-thick Au case, which surrounds a low-density (15 mg/cm^3) CH foam extending from a radius of 2.6 mm to 7.0 mm. The ions for the most part penetrate the Au case and deposit the bulk of their energy in the foam. The

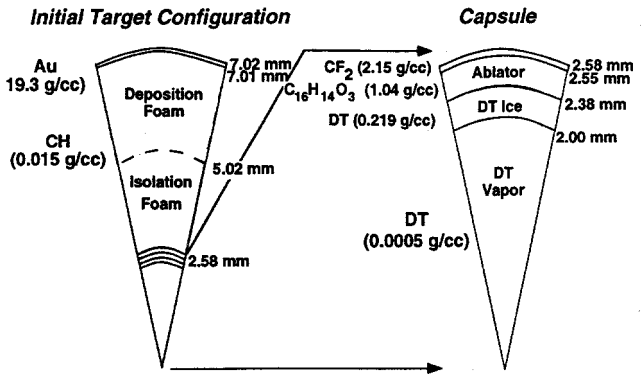

Fig. 1. Schematic illustration of initial target configuration for LIBRA-SP.

capsule contains a 5 mg layer of DT ice, surrounded by a polycarbonate ablator and a 29 μm-thick CF_2 x-ray pulse-shaping[4] layer. The target is driven to implosion by a Li beam profile consisting of a 40 ns, 20 MeV, 26 TW foot, ramping up to a 14 ns, 30 MeV, 480 TW main power pulse. Details of the target design and implosion dynamics will be presented elsewhere.[1]

The total DT fusion yield in the simulation was 552 MJ. Essentially all of the charged particle yield (110 MJ) and 9.1% of the 14.1 MeV neutron yield were reabsorbed in the target. By comparison, detailed neutron transport calculations (see Sec. IV) using density and source term profiles from BUCKY-1 predict that 10.1% of the 14.1 MeV neutrons are reabsorbed. This suggests the relatively simple escape probability model used in BUCKY-1 to compute neutron reabsorption is reasonably accurate.

The energy partitioning within the target is summarized in Fig. 2, where the electron and ion internal energy, kinetic (hydrodynamic) energy, and energy lost due to escaping radiation are shown as a function of time. During the DT burn phase ($t \approx 55.7 - 55.9$ ns), energy is deposited primarily within the fuel, producing a high-temperature, rapidly expanding DT region. This can also be seen in Fig. 3, where the Lagrangian zone boundaries are plotted as a function of time. Note that at early times ($t \approx 56$ ns) up to 75% of the energy contained within the target ($\sim$ 125 MJ, or 23% of the total yield) is in a form of kinetic energy, almost all of which is in the DT and ablator. As the shock propagates out through the ablator and foam, the total kinetic energy decreases. Also during this time, temperatures and internal energies drop as the target radiates away a significant fraction of its energy.

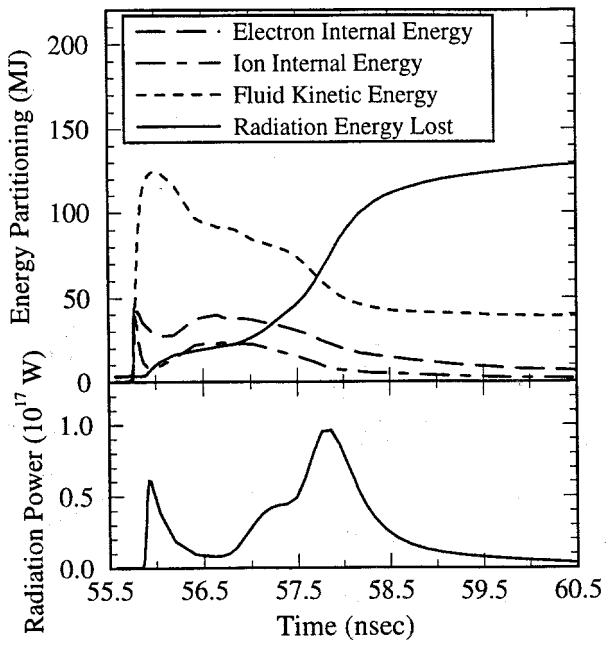

Fig. 2. (Top) Energy partitioning vs. simulation time. The fusion burn phase occurs between $t = 55.7$ and 55.9 ns. (Bottom) Time dependence of x-ray radiation power escaping the target.

The bottom plot in Fig. 2 shows that the x-ray power radiated from the target comes primarily in two bursts. At early times, a hard x-ray component ($h\nu \gtrsim 10$ keV) from the hot DT escapes through the outer layers of the target. This is also shown in Fig. 4, where the frequency-dependent x-ray energy losses, time-integrated up to several simulation

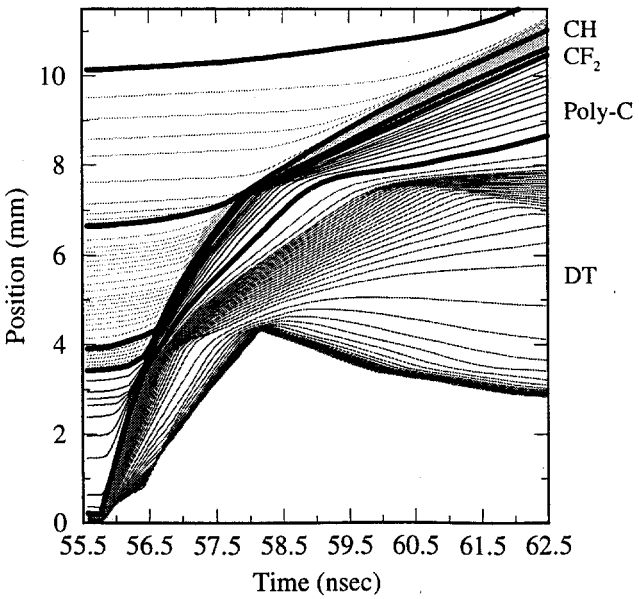

Fig. 3. Lagrangian zone boundary conditions vs. time. The thick solid curves indicate the interfaces between different materials.

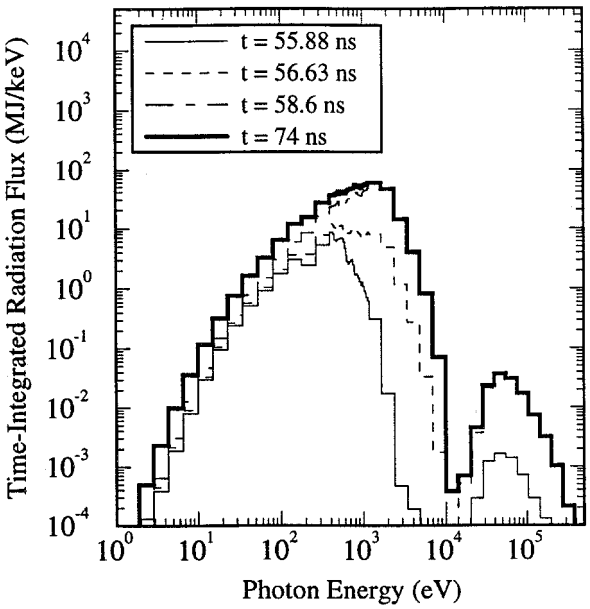

Fig. 4. Frequency dependence of radiation energy emitted from the target. Results are time-integrated up to simulation times shown.

times, are shown. Here, it is seen that virtually all of the x-ray emission above 10 keV is emitted within the first nanosecond after the burn. The power emitted near $h\nu \approx 10$ keV is significantly reduced due to L-shell absorption in the Au case.

The bulk of the radiative energy from the target is emitted at lower photon energies. This occurs as radiation is emitted from the Au case. The peak in the radiation power occurs at approximately 2 ns after the burn phase is completed ($t \sim 57.8$ ns). By 4 ns after burn, roughly 75% of the α particle, neutron, and Li beam energy deposited in the target has been radiated away in the form of x-rays. The frequency dependence of the radiation (Fig. 4) shows that the bulk of the radiation emitted from the target occurs at photon energies of 0.4–3 keV.

By the end of the simulation approximately 40 MJ remains in the form of debris ion kinetic energy. The Au ions carry 82% of this energy, moving at a mean velocity of 7.5×10^7 cm/s (corresponding to Au ions with an energy of 580 keV). These relatively low energy ions are readily stopped in the He target chamber background gas, which is used to provide charge and current neutralization for the Li beam.

IV. TARGET NEUTRONICS SPECTRUM

Neutron fuel interactions in the target result in significant softening of the neutron spectrum as a re-

TABLE I

Target Neutronics Results Per Fusion During Burn

Time Interval	% of Yield	Energy Redeposited (MeV)	Neutrons Emitted
1	5.69	1.992	1.0574
2	12.2	1.992	1.0579
3	23.3	1.717	1.0497
4	15.2	1.469	1.0426
5	10.0	1.288	1.0375
6	7.17	1.184	1.0347
7	5.56	1.114	1.0330
8	4.56	1.055	1.0316
9	3.83	0.984	1.0297
10	3.20	0.890	1.0271
11	2.68	0.787	1.0242
12	2.18	0.687	1.0212
13	4.44	0.524	1.0162
Total	100	1.429	1.0417

sult of elastic and inelastic collisions with the target constituent materials. In addition, neutron multiplication occurs as a result of (n,2n) and (n,3n) reactions and gamma photons are produced. The energy deposited by the neutrons and gamma photons heats the target and ultimately takes the form of radiated x-rays from the hot plasma and expanding ionic debris. Neutronics calculations have been performed for the LIBRA-SP target using the one-dimensional discrete ordinates code ONEDANT.[6] The neutronics calculations performed previously for the LIBRA-SP target used a single configuration at ignition.[2] The previous target calculations also assumed a uniform density in each of the five material regions of the target and the 14.1 MeV fusion neutron source was distributed uniformly in the DT fuel zone. In this work, detailed results of the hydrodynamics calculations are utilized to perform target neutronics calculations that take into account the varying configuration during the burn as well as the distributed material densities and fusion neutron source profile. Calculations have been performed for thirteen time intervals during the burn. The results were combined weighted by the percentage of the yield produced in each time interval to determine the time-integrated overall target neutronics parameters. The calculations were performed using spherical geometry and 46 neutron – 21 gamma group cross section data based on the FENDL-1 nuclear data evaluation.[12]

The total neutron energy reabsorbed in the target is given in Table I for the different time intervals.

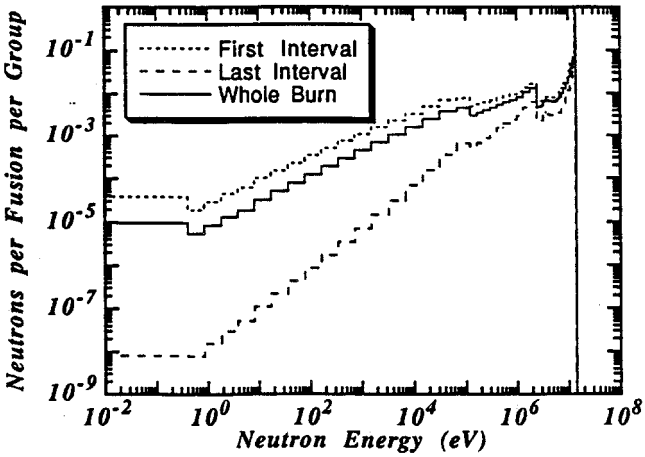

Fig. 5. Energy spectrum of neutrons emitted from the LIBRA-SP target.

The table also includes the number of neutrons emitted from the target per DT fusion. It is clear that due to the reduction in the DT density during the final stages of the burn, the energy deposition and the neutron multiplication decrease. These processes produce a harder neutron spectrum in the final stages of the burn. For example, 86.6% of the emitted neutrons are uncollided 14.1 MeV neutrons in the last interval compared to only 59.9% in the first interval. The overall target neutronics parameters are discussed below.

Due to (n,2n) and (n,3n) reactions occurring in the target, 1.042 neutrons are emitted from the target for each DT fusion reaction. These neutrons carry a total energy of 12.29 MeV implying that the average energy of neutrons emitted from the target is 11.8 MeV. It is interesting to note that only 69.64% of the neutrons emitted from the target are uncollided 14.1 MeV neutrons. For each DT fusion reaction, 0.0033 gamma photons are emitted from the target with an average energy of 3.66 MeV. The energy spectrum of neutrons emitted from the LIBRA-SP target is shown in Fig. 5. The results are shown for the first and last time intervals in addition to the time integrated spectrum over the whole burn.

The total energy deposited by neutrons in the target was calculated to be 1.43 MeV per DT fusion. This corresponds to 10.1% of the original energy carried by fusion neutrons. Almost all of the energy is deposited in the DT fuel zone. Energy deposited by gamma photons is only 133 eV/DT fusion. When the 3.5 MeV energy carried by the alpha particle emerging from the fusion reaction is added, a total energy

TABLE II

Energy Partitioning from LIBRA-SP Target

Neutrons	69.8%
Gamma photons	0.07%
X-rays	22%
Debris Ions	6%
Endoergic loss	2.1%

of 4.93 MeV per DT fusion is found to be carried by x rays and target debris following the microexplosion. Performing an energy balance for the target indicates that 0.371 MeV of energy is lost in endoergic reactions per DT fusion. The detailed partitioning of the energy produced from the target is listed in Table II.

SUMMARY

We have performed radiation-hydrodynamics and neutron transport simulations to investigate the explosion dynamics of a high-gain indirect-drive ICF target. For the LIBRA-SP target configuration studied, our calculations predict a total yield of 552 MJ, providing a gain of approximately 70. Of the total yield, approximately 70% of the energy is carried away by neutrons. The neutron transport calculations indicate a significantly softer spectrum occurs during the early part of the burn phase due to the relatively high fuel densities. About 22% of the target yield is emitted in the form of x rays. Most of this occurs at photon energies of 0.4 – 3 keV. Debris ion kinetic energy accounts for 6% of the total target energy release. Simulations of the type described in this paper are being performed to provide realistic predictions of high-gain ICF target emissions for the purpose of designing a target chamber for ICF power reactors and single-shot test facilities.

ACKNOWLEDGEMENT

This work has been supported in part by Sandia National Laboratories and by Forschungszentrum Karlsruhe, FRG.

REFERENCES

1. R. E. Olson, et al., in preparation (1996).

2. G. L. Kulcinski, et al., "Evolution of Light Ion Driven Power Plants Leading to the LIBRA-SP Design," *Fusion Technology* **26**, 849 (1994).

3. D. R. Welch and C. L. Olson, "Self-Pinched Transport for Ion-Driven ICF," Symposium on Heavy Ion Inertial Fusion, Princeton, NJ (Sept. 1995). C. L. Olson, *J. Fusion Energy* **1**, 309 (1982).

4. R. E. Olson, M. G. Mazarakis, and C. L. Olson, *Fusion Technology* **26**, 922 (1994). R. E. Olson, Symposium on Heavy Ion Inertial Fusion, Princeton, NJ (Sept. 1995).

5. J. J. MacFarlane, G. A. Moses, and R. R. Peterson, "BUCKY-1 — A 1-D Radiation-Hydrodynamics Code for Simulating Inertial Confinement Fusion High Energy Density Plasmas," University of Wisconsin Fusion Technology Institute Report UWFDM–984 (August 1995).

6. R. O'Dell et al., "User's Manual for ONEDANT: A Code Package for One-Dimensional, Diffusion-Accelerated, Neutral Particle Transport," Los Alamos National Laboratory, LA-9184-M, 1989.

7. G. A. Moses, G. Magelssen, R. Israel, T. Spindler, and B. Goel, "PHD-IV – A Plasma Hydrodynamics, Thermonuclear Burn, Radiative Transfer Computer Code," University of Wisconsin Fusion Technology Institute Report UWFDM–194 (August 1985).

8. G. A. Moses, R. R. Peterson, and T. J. McCarville, *Comput. Phys. Commun.* **36**, 249 (1985).

9. R. R. Peterson, J. J. MacFarlane, and G. A. Moses, "CONRAD — A Combined Hydrodynamics-Condensation/Vaporization Computer Code," University of Wisconsin Fusion Technology Institute Report UWFDM–670 (July 1988).

10. "SESAME: The Los Alamos National Laboratory Equation of State Database," LANL Report LA-UR-92-3407, edited by S. P. Lyon and J. D. Johnson (1992).

11. P. Wang, "EOSOPA – A Code for Computing the Equations of State and Opacities of High Temperature Plasmas with Detailed Atomic Models," University of Wisconsin Fusion Technology Institute Report UWFDM–933 (December 1993).

12. R. MacFarlane, "FENDL/MG-1.0, Library of Multigroup Cross Sections in GENDF and MATXS Format for Neutron-Photon Transport Calculations," Summary Documentation by A. Pashchenko, H. Wienke and S. Ganesan, Report IAEA-NDS-129 Rev. 3, International Atomic Energy Agency (Nov. 1995).